AAPT PHYSICS EDUCATION | AMERICAN JOURNAL of PHYSICS

Chaos at the amusement park: Dynamics of the TiltAWhirl

R. L. Kautz and Bret M. Huggard

Citation: American Journal of Physics **62**, 59 (1994); doi: 10.1119/1.17742
View online: http://dx.doi.org/10.1119/1.17742
View Table of Contents: http://scitation.aip.org/content/aapt/journal/ajp/62/1?ver=pdfcov
Published by the American Association of Physics Teachers

frequency interval ($0.98 < f < 1.06$ Hz) even three different modes can be observed with one driving frequency: We get tristability. The dotted parts of the tuning curve again are unstable branches which cannot be observed as stable modes of oscillation. To achieve the oscillations corresponding to the third branch—the upper one—we release the pendulum from a displacement of about 150° antiphase to the driving torque. Since the oscillations are approximately in phase with frequencies below the natural frequency and approximately antiphase with frequencies above it there exist two modes with antiphase. If two pendula are arranged it is fascinating to observe two oscillations with nearly the same phase and two extremely different amplitudes resulting from the same driving torque.

D. Transition to chaotic behavior

With both forms of the restoring torque the transition into chaotic behavior can be demonstrated if the drive torque is increased further (crank arm > 6 cm). We recommend starting the experiment with a frequency well below or well above the natural one. In both cases we get regular oscillations. If we change the frequency and approximate the region of the natural frequency, the amplitude increases. If, finally, the displacement exceeds 180°, we get a turnover which initiates chaotic and irregular movements. If, as recommended before, two identical pendula are used it is most impressive to observe the transition from regular identical movements of both pendula to irregular and noncorrelated movements. In all former experiments regular behavior prevailed—the pendula behaved similarly or in a well-defined relation regarding phase and amplitude. In the chaotic state there is no simple relation and no predictability.

The experiments described above can also be mapped in phase space. To do this Esperidiao *et al.*[7] manipulated a beam of light with the axle of the pendulum. By means of a thread wound around the axle a card was moved up and down thus regulating the quantity of light passing. The light beam was registered by a photoresistor and transformed into electrical values which allowed one to register position and velocity simultaneously and to show the movements in phase space on an oscilloscope.

III. CONCLUSION

A simple mechanical driven oscillator (with a softening and a hardening restoring torque) is described which can be used to demonstrate a variety of nonlinear effects: the bent tuning curve with bistability and the jump effect; a double bent tuning curve with tristability; finally the transition from regular oscillations to chaotic movements. The experiments can be well observed by a large audience but may also be used as individual lab experiments.

[1]R. Khosropour and P. Millet, "Demonstrating the bent tuning curve," Am. J. Phys. **60**, 429–432 (1992).

[2]A. B. Pippard, *The Physics of Vibration*, Vol. 1 (Cambridge University, New York, 1978), pp. 247–253.

[3]I. G. Pain, *Vibrations and Waves in Physics*, 2nd ed. (Cambridge University, New York, 1984), Chap. 7.

[4]J. A. Elliott, "Intrinsic nonlinear effects in vibrating strings," Am. J. Phys. **48**, 478–480 (1980).

[5]N. B. Tuffilaro, "Nonlinear and chaotic string vibrations," Am. J. Phys. **57**, 408–414 (1989).

[6]B. Hoke, "Nonlinearity in rubber band vibrations," Senior thesis, Hamilton College, Clinton, New York, 1990.

[7]A. S. C. Esperidiao, G. P. Guedes, K. Weltner, and R. F. S. Andrade, "Espaco de fase do pendulo fisico nao linear: Experimentos e integracao numerica," Rev. Bras. Ensino Fis. **14**, 78–86 (1992).

Chaos at the amusement park: Dynamics of the Tilt-A-Whirl

R. L. Kautz[a] and Bret M. Huggard

Department of Physics and Astronomy, Northern Arizona University, Flagstaff, Arizona 86011

(Received 8 March 1993; accepted 29 June 1993)

Analysis of the dynamics of an amusement-park ride reveals that the passengers experience chaotic motion.

I. INTRODUCTION

During the past decade, chaotic behavior has been discovered in a wide range of dynamical systems governed by simple deterministic equations.[1,2] Chaotic motion is now understood to explain a variety of apparently random phenomena from dripping faucets[3] to the irregular rotation of a moon of Saturn.[4] Chaos is also found occasionally in commercial products. In particular, certain toys derive their fascination from the unpredictable nature of chaotic motion. Although the designers probably employed chaos unwittingly, mathematical analysis of two such toys reveals the presence of genuine chaotic behavior.[5,6] For the physics lecturer, these toys provide readily available examples of chaotic motion suitable for classroom demonstrations.

In this paper, we investigate another commercial application of chaos that allows the pseudorandom motion of a deterministic system to be experienced directly. Specifically, we analyze the dynamics of an amusement-park ride called the Tilt-A-Whirl. A passenger on the Tilt-A-Whirl rides in one of seven identical cars, each of which is free to pivot about the center of its own circular platform. The platforms move along a hilly circular track that tilts the platforms in all possible directions. Although the translation and tilting of the platforms are completely regular, the

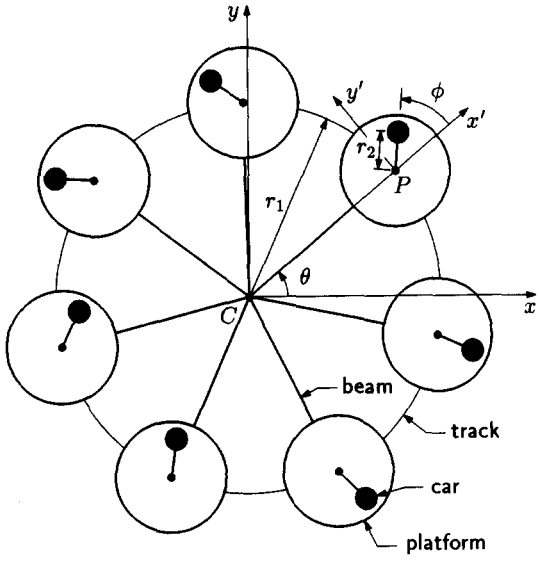

Fig. 1. Plan view of the idealized Tilt-A-Whirl.

cars whirl around in an independent and apparently irregular manner. The ride is fun because you never know exactly what will happen. As your car rides up and down the next hill, it may spin clockwise, counterclockwise, or hesitate without spinning at all.

Is the motion of a Tilt-A-Whirl car another example of deterministic chaos? To answer this question, we have developed a mathematical model for the Tilt-A-Whirl and simulated its motion on a computer. The equation of motion for a single car, derived from Lagrange's equation, is that of a damped pendulum with a periodically rotating equilibrium angle. When this equation is integrated numerically, we find steady-state motion in which the car moves with the same irregular, apparently unpredictable whirling as the actual ride. Thus, the pseudorandom motion of the Tilt-A-Whirl and the surprises that make the ride exciting are almost certainly a direct product of deterministic chaos. Given this fact, a ride on the Tilt-A-Whirl can provide students of physics with a new appreciation for chaotic behavior.

The Tilt-A-Whirl was invented by Herbert W. Sellner in 1926 and first operated at an amusement park in White Bear Lake, MN. Because the possibility of deterministic chaos was not widely understood at that time (although Poincaré had established the fundamentals before the turn of the century),[7] it is safe to assume that Sellner discovered the surprising dynamics of his machine by building one, rather than by mathematical analysis. However, the geometry of the Tilt-A-Whirl is sufficiently simple that we can easily derive an approximate equation of motion. As a first step in this derivation, we describe a geometric idealization of the Tilt-A-Whirl mechanism.

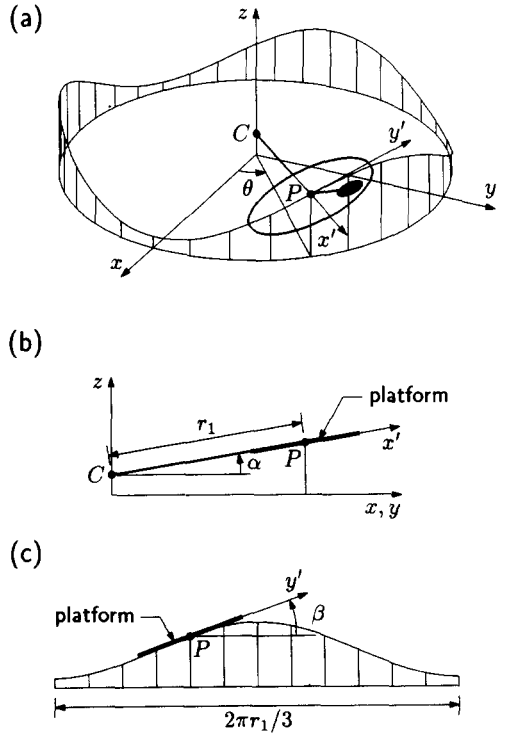

Fig. 2. (a) Perspective view of the Tilt-A-Whirl showing the track and a single platform. (b) Vertical cross section of the Tilt-A-Whirl taken through points C and P. (c) Vertical cross section of the Tilt-A-Whirl taken through point P and tangent to the circular track. In part (c), one-third of the track is shown unrolled in the tangent plane. In all parts of the figure, vertical dimensions are exaggerated by a factor of 2.

II. IDEALIZED GEOMETRY

A plan view of the idealized Tilt-A-Whirl is shown in Fig. 1. The machine includes seven circular platforms that are driven at a uniform speed along a circular track which includes three identical hills. Each platform is rigidly attached to a beam connected to the center C of the machine through a ball joint. The distance from C to the center P of a platform is r_1, and we assume that the track is of the same radius. On each platform, a wheeled car is attached at point P, which acts as a pivot point about which the car is free to rotate. Because the center of mass of the car is offset from the pivot point, a car is represented in Fig. 1 as a pendulum with a moment arm of length r_2. Since the wheels of a car are always in contact with the platform, the pendulum is confined to the plane of the platform.

In deriving an equation of motion, we represent the car by a point mass located at its center of gravity. To apply Lagrange's equation, we must first determine the coordinates (x,y,z) of this point mass in terms of the angle θ which defines the location of the platform and the angle ϕ which defines the location of the mass on the platform. The relevant three-dimensional geometry is illustrated in Fig. 2(a) which shows the Tilt-A-Whirl track and one platform in perspective. In our idealized geometry, the platform is tangent to the track at point P, and the height of point P varies sinusoidally as the platform moves around the track. Due to constraints imposed by the beam and the track, the location and tilt of the platform are completely determined by the angle θ.

To aid in the analysis, we introduce a coordinate system (x',y') attached to the platform and define angles α and β to describe the tilt of the platform. The origin of the (x',y') coordinate system is the pivot point P and the x' axis is taken to be an extension of the line from C to P. As shown in Figs. 2(b) and 2(c), α and β are the angles of the x' and y' axes with respect to the x–y plane. In the (x',y') coordinate system, the position of the point mass representing the car is

$$x' = r_2 \cos\phi, \tag{1}$$

$$y' = r_2 \sin\phi, \tag{2}$$

as shown in Fig. 1. In the (x,y,z) coordinate system, the location of point P is given by

$$x_P = r_1 \cos\alpha \cos\theta, \tag{3}$$

$$y_P = r_1 \cos\alpha \sin\theta, \tag{4}$$

$$z_P = z_C + r_1 \sin\alpha, \tag{5}$$

where z_C is the height of point C. Finally, the position of the car in the (x,y,z) system can be written as

$$x = x_P + x'\cos\alpha\cos\theta - y' \times(\cos\beta\sin\theta + \sin\alpha\sin\beta\cos\theta), \tag{6}$$

$$y = y_P + x'\cos\alpha\sin\theta + y' \times(\cos\beta\cos\theta - \sin\alpha\sin\beta\sin\theta), \tag{7}$$

$$z = z_P + x'\sin\alpha + y'\cos\alpha\sin\beta. \tag{8}$$

Taken together, Eqs. (1)–(8) specify the position of the car's center of mass in terms of α, β, θ, and ϕ.

It remains to express α and β in terms of θ. To obtain simple expressions for α and β, we note that, because neither angle exceeds 10°, the small-angle approximations $\sin\alpha = \tan\alpha = \alpha$ and $\sin\beta = \tan\beta = \beta$ can be applied without significant error. In this case, the height of the track is approximately $z_P = z_C + r_1\alpha$, and the required sinusoidal variation in z_P is obtained by choosing

$$\alpha = \alpha_0 - \alpha_1 \cos 3\theta, \tag{9}$$

where α_0 and α_1 are constants. Equation (9) specifies the shape of the idealized track, including three identical hills, as shown in Fig. 2(a). From Fig. 2(c) it can be seen that $\beta = (1/r_1)dz_P/d\theta$, so that

$$\beta = 3\alpha_1 \sin 3\theta. \tag{10}$$

Thus, the tilt angles α and β both oscillate sinusoidally with θ and complete three oscillations as the platform makes one circuit of the track.

III. EQUATION OF MOTION

Equations (1)–(10) provide all of the geometric information required to derive an equation of motion for the Tilt-A-Whirl. These equations allow the coordinates (x,y,z) of the point mass representing the car to be expressed in terms of θ and ϕ. The final information required is the kinematic relation

$$\theta = \omega t, \tag{11}$$

which states that the position angle of the platform advances uniformly in time. Using Eqs. (1)–(11), we can express (x,y,z) in terms of ϕ and t. Thus, the Tilt-A-Whirl is a time-dependent dynamical system with a single degree of freedom, the position angle ϕ of the car. The equation of motion to be derived specifies how ϕ changes with time.

The form of Lagrange's equation appropriate to the Tilt-A-Whirl is

$$\frac{d}{dt}\left(\frac{\partial T}{\partial \dot\phi}\right) - \frac{\partial T}{\partial \phi} = -\frac{\partial V}{\partial \phi}, \tag{12}$$

where T is the kinetic energy of the car

$$T(\phi,\dot\phi,t) = \frac{m}{2}(\dot x^2 + \dot y^2 + \dot z^2), \tag{13}$$

and V is the gravitational potential energy of the car

$$V(\phi,t) = mgz. \tag{14}$$

In these equations, m is the mass of the car, g is the acceleration of gravity, and dots have been used to denote the time derivatives of x, y, z, and ϕ.

In principle, Eqs. (1)–(14) might be combined without further approximation to derive an equation of motion for ϕ. In order to obtain a reasonably simple result, however, we again use the fact that the angles α and β are small. When we omit all terms of quadratic or higher order in α and β, Eq. (12) reduces to

$$mr_2^2\frac{d^2\phi}{dt^2} + mr_1r_2\omega^2\sin\phi = mgr_2(\alpha\sin\phi - \beta\cos\phi). \tag{15}$$

The terms in this equation of motion are easily identified. The first term on the left is the moment of inertia of the car times its angular acceleration. The second term on the left is the torque on the car due to the centrifugal force generated by the rotation of the platform about the center of the machine. The term on the right is the gravitational torque on the car due to the tilt of the platform.

While Eq. (15) represents a good approximate equation for the Tilt-A-Whirl in the absence of friction, the actual machine is far from frictionless. To account for losses, we introduce a torque proportional to $d\phi/dt$ that represents the effect of viscous damping on the car. With this term included, the equation of motion becomes

$$mr_2^2\frac{d^2\phi}{dt^2} + \rho\frac{d\phi}{dt} + mr_1r_2\omega^2\sin\phi - mgr_2 \times(\alpha\sin\phi - \beta\cos\phi) = 0, \tag{16}$$

where ρ is the damping coefficient. This equation combined with Eqs. (9)–(11) defines the motion of the idealized Tilt-A-Whirl to be studied here. Because α and β vary sinusoidally with time and the $\sin\phi$ and $\cos\phi$ terms are nonlinear, Eq. (16) can be classified as a time-dependent nonlinear ordinary differential equation. The nonlinearity of Eq. (16) is essential to the present problem, since the chaotic motion that makes the Tilt-A-Whirl interesting can only occur in a nonlinear system.

As Eqs. (9)–(11) and (16) reveal, the dynamics of the Tilt-A-Whirl is determined by six parameters: r_1, r_2, α_0, α_1, ω, and ρ/m. Four of these parameters, r_1, α_0, α_1, and ω, are easy to measure accurately. For the machines now in operation, $r_1 = 4.3$ m, $\alpha_0 = 0.036$ rad, $\alpha_1 = 0.058$ rad, and $\omega/2\pi = 6.5$ rpm. However, the moment arm r_2 depends on the mass distribution of the car and riders, which is poorly known. The nominal value of 0.8 m adopted here for r_2 is thus only an estimate. The ratio ρ/m is also difficult to determine accurately but, as we show in the next section, an estimate can be obtained from the quality factor of the car's natural oscillations.

IV. FIXED-PLATFORM DYNAMICS

Before discussing the chaotic motion of the driven Tilt-A-Whirl, we explore the dynamics of the car when the platform on which it rolls is stationary. An examination of

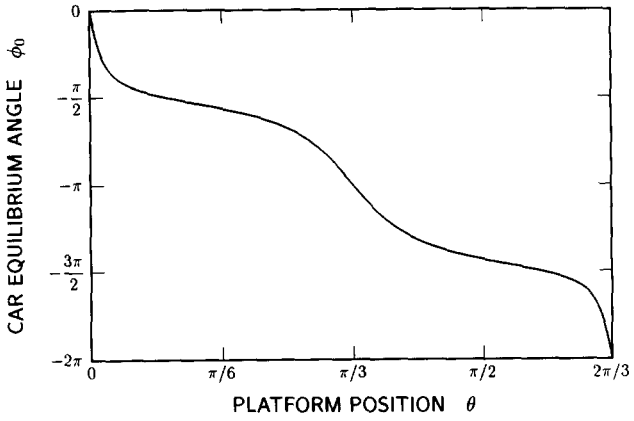

Fig. 3. Car equilibrium angle as a function of platform position. This function is defined by Eqs. (9), (10), and (19) with $\alpha_0=0.036$ rad and $\alpha_1=0.058$ rad.

this case provides further insight into the dynamical properties of the Tilt-A-Whirl. When the drive is turned off, the angle θ is fixed, and the motion of a car is described by the equation

$$mr_2^2\frac{d^2\phi}{dt^2}+\rho\frac{d\phi}{dt}-mgr_2(\alpha\sin\phi-\beta\cos\phi)=0, \quad (17)$$

where α and β are fixed angles determined by Eqs. (9) and (10). This equation can also be written in the form

$$mr_2^2\frac{d^2\phi}{dt^2}+\rho\frac{d\phi}{dt}+mgr_2\sqrt{\alpha^2+\beta^2}\sin(\phi-\phi_0)=0, \quad (18)$$

where ϕ_0 is defined by

$$\sin\phi_0=-\beta/\sqrt{\alpha^2+\beta^2},\quad \cos\phi_0=-\alpha/\sqrt{\alpha^2+\beta^2}. \quad (19)$$

Equation (18) describes the motion of a car as it comes to rest after the platform stops. This equation is equivalent to that of a commonly studied system: the damped pendulum. Given this equivalence, we expect the car to display damped oscillations as it approaches its equilibrium position. In this case, the equilibrium angle is ϕ_0. Considering small displacements from ϕ_0, it can be shown that the natural oscillation frequency of a car is

$$\omega_0=\sqrt{g/r_2}(\alpha^2+\beta^2)^{1/4}. \quad (20)$$

Thus, the natural frequency depends on the tilt of the platform as defined by α and β. While this formula is not valid for large values of tilt, we note that $\sqrt{g/r_2}$ is the natural frequency of a pendulum with a horizontal axis of rotation. For the nominal values of α_0 and α_1 given in Sec. III, the factor $(\alpha^2+\beta^2)^{1/4}$ varies between 0.148 and 0.422. Thus, the oscillation period $2\pi/\omega_0$ of the car can be anything from about 4 to 12 s, depending on the tilt of the platform.

The damping of a pendulum is often expressed in terms of the quality factor Q, defined as the ratio of the energy stored in the pendulum to the energy dissipated during one oscillation. For the pendulum described by Eq. (18), the quality factor is

$$Q=Q_0(\alpha^2+\beta^2)^{1/4}, \quad (21)$$

where the parameter Q_0 is defined as

$$Q_0=(m/\rho)\sqrt{gr_2^3}. \quad (22)$$

For $Q>0.5$ the oscillations are underdamped, and for $Q<0.5$, the oscillations are overdamped. Observation of the Tilt-A-Whirl reveals that the car is underdamped but its oscillations decay rapidly, which suggests that the damping corresponds roughly to $Q_0=20$. Allowing for the variation of $(\alpha^2+\beta^2)^{1/4}$ in Eq. (21), $Q_0=20$ implies a range of Q between about 3.0 and 8.4, depending on the tilt of the platform. Because ρ/m is related to Q_0 and r_2 by Eq. (22), specifying $Q_0=20$ fixes ρ/m, the final Tilt-A-Whirl parameter to be determined.

V. CHAOTIC DYNAMICS

Suppose now that the platform moves very slowly along the track so that the centrifugal force on the car is negligible. In this case, the car will remain near its equilibrium position ϕ_0 and rotate slowly as the tilt of the platform changes. How does ϕ_0 vary with θ? Combining Eqs. (9), (10), and (19), we plot ϕ_0 as a function of θ in Fig. 3. At $\theta=0$, the platform is located at the bottom of a valley and tilts away from the center of the machine. Thus, as Fig. 2(a) suggests, $\phi_0=0$ at $\theta=0$, and the equilibrium position coincides with the x' axis. As θ increases and the platform begins to climb the first hill, the equilibrium point rotates toward the negative y' axis, and ϕ_0 becomes negative. When the platform reaches the top of the hill at $\theta=\pi/3$, it tilts toward the center of the machine and $\phi_0=-\pi$. As the platform moves down the far side of the hill, the equilibrium angle swings toward the positive y' axis, and ϕ_0 continues to rotate in the negative ϕ direction until it reaches $\phi_0=-2\pi$ at the bottom of the valley. Thus, the equilibrium angle completes exactly one backward revolution as the platform moves from the bottom of one valley to the bottom of the next. When ω is small and the platform moves slowly, the car will follow the same motion, rotating backward by one revolution as it passes over each hill.

In the limit of large ω, on the other hand, the centrifugal term dominates the gravitational term, and the car is forced to the outer edge of the platform. In this case, the position of the car is always near $\phi=0$ and there is no rotation with respect to the (x',y') coordinate system. Mathematically, this situation is approximated by neglecting the gravitational term in Eq. (16), and the dynamics are roughly described by

$$mr_2^2\frac{d^2\phi}{dt^2}+\rho\frac{d\phi}{dt}+mr_1r_2\omega^2\sin\phi=0. \quad (23)$$

Again, we find an equation equivalent to that of a damped pendulum but in this case the equilibrium angle is $\phi=0$. Thus, as expected intuitively, the car is forced to the outer edge of the platform and remains there indefinitely when ω is large.

At this point, it is natural to ask what happens at intermediate values of ω. That is, what motion does the car assume in the transition region between low speeds, where it rotates one revolution backward in going over each hill, and high speeds, where it is locked at the outer edge of the platform? To answer this question, we turn to numerical simulations and introduce for this purpose a dimensionless form of the equation of motion. If we define the dimensionless parameters τ, γ, and ϵ by

$$\tau=3\omega t, \quad (24)$$

$$\gamma=(1/3\omega)\sqrt{g/r_2}, \quad (25)$$

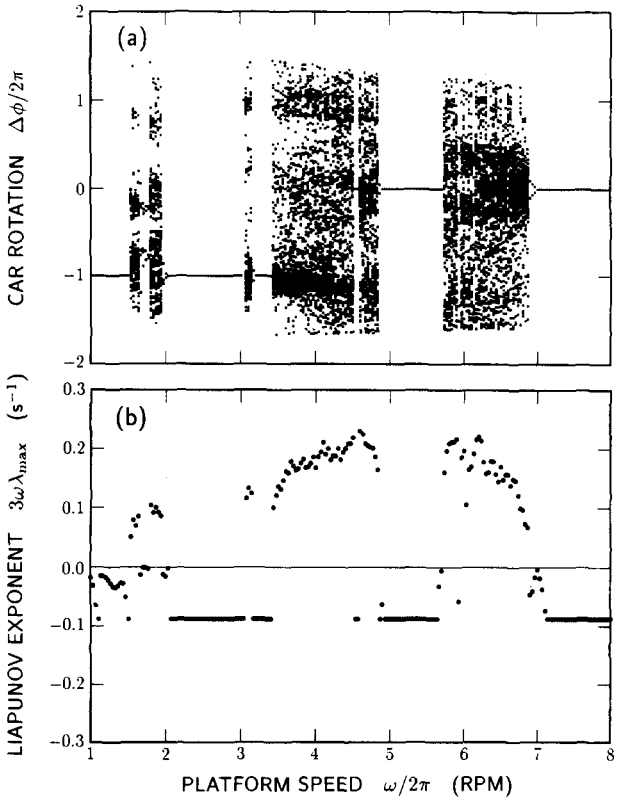

Fig. 4. (a) Scatter plot of the net rotation $\Delta\phi$ per tilt cycle as a function of platform speed for $r_1=4.3$ m, $r_2=0.8$ m, $\alpha_0=0.036$ rad, $\alpha_1=0.058$ rad, and $Q_0=20$. At each speed, the equation of motion is integrated for 1000 tilt cycles to eliminate transients and then a dot is plotted for each $\Delta\phi$ recorded during the next 100 tilt cycles. (b) Maximum Liapunov exponent as a function of platform speed for the same parameters as in part (a). Exponents were calculated over an interval of 1000 tilt cycles after transients were eliminated.

$$\epsilon=r_1/9r_2, \tag{26}$$

then Eq. (16) becomes

$$\frac{d^2\phi}{d\tau^2}+(\gamma/Q_0)\frac{d\phi}{d\tau}+(\epsilon-\gamma^2\alpha)\sin\phi+\gamma^2\beta\cos\phi=0, \tag{27}$$

where

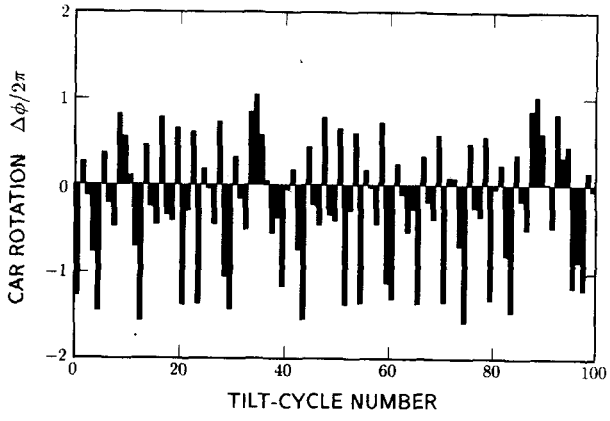

Fig. 5. Net rotation $\Delta\phi$ per tilt cycle as a function of cycle number for the same paramters as in Fig. 4 with $\omega/2\pi=5.9$ rpm.

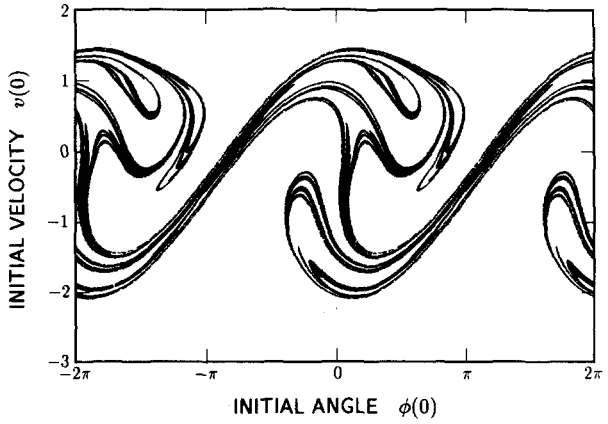

Fig. 6. Poincaré section of a chaotic trajectory for the same parameters as in Fig. 4 with $\omega/2\pi=5.9$ rpm. A single point is plotted to mark the angle ϕ and angular velocity v of the car at the beginning of each of 100 000 successive tilt cycles. The Poincaré section is plotted over a 4π interval in ϕ to reveal its cyclic nature.

$$\alpha=\alpha_0-\alpha_1\cos\tau, \tag{28}$$

$$\beta=3\alpha_1\sin\tau. \tag{29}$$

In this equation, the parameter τ is the time normalized to $1/3\omega$, and the platform advances over one hill as τ increases by 2π. Because the time-dependent coefficients in Eq. (27) both have a period of $\Delta\tau=2\pi$, this period is more relevant to the motion of the car than the time required to complete a circuit of the track. Thus, in the following analysis, we focus on what happens to the car each time the platform advances from the bottom of one valley to the bottom of the next.

Since the tilt of the platform cycles through the same values each time it traverses a hill, we expect that the steady-state motion of the car will typically assume the same periodicity. That is, we expect to find solutions for which

$$\phi(\tau+2\pi)=\phi(\tau)+2\pi n \tag{30}$$

for all τ, where n is an integer. For such solutions, the car advances by n revolutions during each tilt cycle. The asymptotic solutions for both small and large ω fall into this category. For small ω the car rotates backward one revolution during each tilt cycle and $n=-1$, while for large ω there is no rotation and $n=0$. To describe more general solutions, we define the car rotation on the mth tilt cycle by

$$\Delta\phi(m)=\phi(2\pi m)-\phi[2\pi(m-1)]. \tag{31}$$

For solutions that satisfy Eq. (30), the rotation is the same during every tilt cycle. For chaotic solutions, on the other hand, we expect $\Delta\phi$ to vary from cycle to cycle in an irregular and apparently unpredictable way.

Using the car rotation per tilt cycle as a guide, we now investigate the behavior of the Tilt-A-Whirl at intermediate values of ω. Figure 4(a) is a scatter plot of $\Delta\phi$ as a function of the platform speed. For each ω considered in this figure, the equation of motion was integrated for 1000 tilt cycles to eliminate transients and then the next 100 values of $\Delta\phi$ were plotted as discrete points. The values of rotation plotted in Fig. 4(a) thus characterize the steady-state solution at each platform speed. At small ω, the steady-state rotation is identically -2π, as expected on the

basis of our quasistatic analysis. Similarly, at large ω, the rotation is identically 0 because the car is locked at the outer edge of the platform. However, at various speeds between about 1.5 and 7 rpm, the rotation varies from cycle to cycle, even after transients are eliminated. At such speeds, Fig. 4(a) reveals $\Delta\phi$ values scattered between roughly -3π and 3π. This scatter represents the kind of chaotic motion that makes the Tilt-A-Whirl fun to ride.

Although the equation of motion used here is only approximate and some Tilt-A-Whirl parameters are not known with certainty, we note that Fig. 4(a) does indicate the presence of chaotic motion at 6.5 rpm, the actual speed of the Tilt-A-Whirl. Thus, in spite of its limitations, our idealized model seems to capture the essence of this ride. At 6.5 rpm, however, the calculated values of car rotation tend to cluster around 0, as Fig. 4(a) suggests. Because the simulation yields more widely scattered values of rotation at 5.9 rpm, we adopt this speed as a more accurate reflection of the machine's actual performance.

Figure 5 plots a typical sequence of car rotations over a period of 100 tilt cycles at 5.9 rpm. Given that a tilt cycle takes only about 3 s, it is not hard to imagine that the apparently random sequence of rotations shown here makes an exciting amusement-park ride. While $\Delta\phi$ is confined to a range of values between roughly -3π and 2π at 5.9 rpm, a passenger can never be certain what will happen next. Frequent but irregular alternations between positive and negative rotation make the Tilt-A-Whirl very lively.

The jumbled mixture of rotations shown in Fig. 5 is entirely characteristic of the steady-state motion. The apparent random element of the motion is not simply a complex initial transient but persists indefinitely. Although there are similarities in the pattern of rotation from time to time, the motion never repeats itself exactly, even over periods greater than 10^5 tilt cycles. At the same time, the apparently random sequence in Fig. 5 is completely predictable in principle because the equation of motion is deterministic. A sequence of this type is often described as pseudorandom to indicate that it includes an element that is random according to statistical tests but has an underlying order that is difficult to perceive. Pseudorandom behavior is one of the identifying characteristics of deterministic chaos.

The ordered aspect of the chaotic motion at 5.9 rpm is suggested by a plot called a Poincaré section, shown in Fig. 6. Because Eq. (27) is second order, a solution is uniquely determined by specifying the initial angle ϕ and angular velocity $v \equiv d\phi/d\tau$ at $\tau=0$. However, the periodicity of the coefficients in Eq. (27) implies the equivalence of all times for which $\tau=0$ modulo 2π. We can thus conveniently track the state of the car by recording ϕ and v at the beginning of successive tilt cycles. In Fig. 6, we use $\phi(0)$ and $v(0)$ to denote the values of ϕ and v at any time $\tau=0$ modulo 2π and plot points $[\phi(0),v(0)]$ corresponding to 100 000 successive tilt cycles of the chaotic solution. The variables $\phi(0)$ and $v(0)$ are state variables defined on a discrete time grid and a point $[\phi(0),v(0)]$ marks the location of the car in state space.

The Poincaré section of a periodic solution having the form given by Eq. (30) consists of a single point, since ϕ and v are the same at the beginning of every tilt cycle. In contrast, the Poincaré section of a chaotic solution includes an infinite number of points. As Fig. 6 shows, these points are not scattered randomly in state space but form a distinctive swirl confined to a small part of the $\phi(0)$-$v(0)$ plane. Thus, while the chaotic state allows a wide range of variation in motion from cycle to cycle, the possibilities are constrained by the dynamical properties of the system. Moreover, the constraint represented by this swirl of points does not depend on initial conditions. If the system is initialized at a point $[\phi(0),v(0)]$ far from the points plotted in Fig. 6, the trajectory converges to the swirl within a few tilt cycles and is thereafter confined to this region. For this reason, the swirl is called a chaotic attractor.

VI. LIAPUNOV EXPONENTS

Given the highly structured character of the chaotic attractor, it may seem surprising that motion within the attractor is irregular. After all, the current values of $\phi(0)$ and $v(0)$ completely determine what the next values will be, so the system must hop from one part of the attractor to another in a predictable way. To understand why this determinism does not lead to regular motion, we now consider how the Tilt-A-Whirl reacts to small perturbations. Our analysis of perturbations will also explain why aficionados of the ride refuse to sit still in their seats.

Suppose we have computed a solution $\phi(\tau)$ and wish to know how this solution is affected by an infinitesimal perturbation occurring at $\tau=0$. The perturbed solution $\phi'(\tau)$ can be written as

$$\phi'(\tau)=\phi(\tau)+\delta(\tau), \tag{32}$$

where $\delta(\tau)$ is the difference between the perturbed solution and the original solution. An equation of motion for δ can be derived using the fact that both ϕ and ϕ' satisfy Eq. (27) for $\tau>0$. Because δ is infinitesimal, the equation can be linearized to yield

$$\frac{d^2\delta}{d\tau^2}+(\gamma/Q_0)\frac{d\delta}{d\tau}+[(\epsilon-\gamma^2\alpha)\cos\phi-\gamma^2\beta\sin\phi]\delta=0, \tag{33}$$

where α, β, and ϕ are known functions of τ.

We now wish to determine whether the effect of the perturbation grows or decays in time. Because Eq. (33) is a second-order linear equation, all possibilities are included if we compute two linearly independent solutions δ_a and δ_b. In particular, we choose solutions with the initial conditions

$$[\delta_a(0),\dot{\delta}_a(0)]=(1,0), \tag{34}$$

$$[\delta_b(0),\dot{\delta}_b(0)]=(0,1), \tag{35}$$

where $\dot{\delta}=d\delta/d\tau$. Information about the growth or decay of δ_a and δ_b is included in the Jacobian matrix $\mathbf{J}$ defined by

$$\mathbf{J}(\tau)=\begin{pmatrix}\delta_a(\tau) & \delta_b(\tau)\\ \dot{\delta}_a(\tau) & \dot{\delta}_b(\tau)\end{pmatrix}. \tag{36}$$

This information is reduced to its essentials by computing the Liapunov characteristic exponents[8]

$$\lambda_i=\lim_{\tau\to\infty}\tau^{-1}\ln\left|i\text{th eigenvalue of }\mathbf{J}(\tau)\right|. \tag{37}$$

Because $\mathbf{J}$ is a two-dimensional matrix, it has two eigenvalues, and there are two characteristic exponents λ_1 and λ_2. As Eq. (37) suggests, the Liapunov exponents measure the average rate at which δ grows, assuming this growth is exponential. Different components of the perturbation

grow or decay as $\exp(\lambda_1\tau)$ and $\exp(\lambda_2\tau)$ in the limit of large time. If λ_1 and λ_2 are both negative, then the perturbation decays and the system quickly returns to its original trajectory. If either exponent is positive, however, then one component of the perturbation grows, and the perturbed solution diverges from the original solution at an exponential rate.

The characteristic exponents of a system are generally constrained by a sum rule.[8] In the present instance, this sum rule is

$$\lambda_1+\lambda_2=-\gamma/Q_0. \tag{38}$$

Thus, knowing the larger of the two characteristic exponents, $\lambda_{\max}=\max(\lambda_1,\lambda_2)$, also defines the smaller exponent $\lambda_{\min}=\min(\lambda_1,\lambda_2)$. According to Eq. (38), $\lambda_{\max}$ can never be less than $-\gamma/2Q_0$, which results when $\lambda_1=\lambda_2$.

Numerically computed values of the maximum Liapunov exponent are plotted as a function of platform speed in Fig. 4(b). In regions where the solution is periodic and the rotation is either 0 or -2π on every tilt cycle, $\lambda_{\max}$ is negative and the car quickly returns to its original trajectory after a perturbation. Indeed, for periodic solutions, $\lambda_{\max}$ often assumes its minimum possible value of $-\gamma/2Q_0$, which corresponds to $3\omega\lambda_{\max}=-0.0875\ \mathrm{s}^{-1}$ in the present case. This minimum of $\lambda_{\max}$ is obtained when the eigenvalues of **J** are complex conjugates of one another and their magnitudes are equal. For platform speeds at which the motion is chaotic, in contrast, $\lambda_{\max}$ is positive and a perturbation causes the car to diverge from its original trajectory at an exponential rate.

The association of a positive Liapunov exponent with chaotic behavior is in fact fundamental. A positive Liapunov exponent implies that two solutions beginning at nearly the same point on the chaotic attractor will diverge exponentially with the passage of time. Both trajectories remain on the attractor but quickly move to well-separated regions of state space. This phenomena, often described as "extreme sensitivity to initial conditions," is a hallmark of chaotic behavior, and a positive exponent is often accepted as proof that the motion is chaotic. A positive exponent also helps to explain the apparent randomness of chaotic motion. That is, even though the passage of one tilt cycle necessarily maps a given point $[\phi(0),v(0)]$ on the chaotic attractor into a specific new point $[\phi_1(0),v_1(0)]$, a positive exponent implies that points relatively close to $[\phi(0),v(0)]$ may not map into points near $[\phi_1(0),v_1(0)]$. Thus, extreme sensitivity to initial conditions makes chaotic motion unpredictable to the casual observer, giving it a pseudorandom quality.

The complex structure of the chaotic attractor is another aspect of chaotic motion related to the positive sign of the Liapunov exponent. In general, chaotic attractors like that shown in Fig. 6 are classified as fractals: intricate geometric objects described by a noninteger dimensionality. While the dimension D of a fractal can be defined in a number of ways, the Liapunov dimension is given by the formula[9]

$$D=1+\lambda_{\max}/|\lambda_{\min}|, \tag{39}$$

which is applicable to the Poincaré section of a chaotic Tilt-A-Whirl trajectory. For the chaotic attractor shown in Fig. 6, we have $\lambda_{\max}=0.113$, $\lambda_{\min}=-0.207$, and $D=1.55$. Thus, in the limit that the number of points plotted in Fig. 6 approaches infinity, we obtain a geometric object having a dimension between that of a line and that of an area. The fractal nature of the chaotic attractor reflects the fact that the steady-state trajectory never repeats and must occupy a sizeable region of state space.

In the preceding analysis, we have assumed that the passengers remain fixed within the car and the only time dependence of the system is the regular variation of the tilt angle of the platform as it moves along the track. As long as the passengers sit still, the Tilt-A-Whirl is deterministic and the observed pseudorandom motion can be considered chaotic. However, many passengers discover that they can affect the motion of the car by throwing their weight from one side to the other at crucial moments. Such actions can change what might have been a tilt cycle with little or no rotation into one with a good whirl. The effectiveness with which a passenger can modify his trajectory in this way is a consequence of the sensitivity of chaotic motion to small perturbations. As indicated in Fig. 4(b), the Liapunov exponent at 5.9 rpm is about $3\omega\lambda_{\max}=0.21\ \mathrm{s}^{-1}$ so that the deviation caused by a perturbation increases on average by a factor of e every 4.8 s. (The factor of 3ω included here restores the dimensions of inverse time to the exponent.) Very probably, perturbations occurring at special times will grow even faster in the short term, making the consequences of a passenger's appropriately timed lunge almost immediate. Thus, it would seem that aficionados of the Tilt-A-Whirl have known for some time that chaotic systems can be controlled using small perturbations, a principle that has recently been applied by scientists to the less frivolous task of suppressing chaotic behavior.[10]

Is the Tilt-A-Whirl unique among amusement-park rides in exploiting chaos to create an unpredictable and exciting ride? A walk around an amusement park suggests that several other common rides display chaotic behavior similar to that of the Tilt-A-Whirl. Such rides typically employ a car with a single degree of freedom driven by a deterministic mechanism. We leave it as a challenge for students to identify other chaotic rides and analyze their motion, in the hope that their next visit to an amusement park will be an educational experience.

ACKNOWLEDGMENTS

The authors are pleased to thank William P. Dubé who first suggested the connection between chaos and amusement-park rides and Bruce A. Sellner for providing engineering drawings of the Tilt-A-Whirl. R.L.K. thanks members of the Department of Physics and Astronomy and the Department of Mathematics for their hospitality during his stay at Northern Arizona University. Bret Huggard was partially supported by an undergraduate research assistantship provided by the NASA Space Grant Consortium Program at Northern Arizona University.

[a]Permanent address: National Institute of Standards and Technology, 325 Broadway, Boulder, Colorado 80303.

[1]F. C. Moon, *Chaotic and Fractal Dynamics: An Introduction for Applied Scientists and Engineers* (Wiley, New York, 1992).

[2]*Exploring Chaos: A Guide to the New Science of Disorder*, edited by N. Hall (Norton, New York, 1993).

[3]R. Shaw, *The Dripping Faucet as a Model Chaotic System* (Ariel, Santa Cruz, 1984); P. Martien, S. C. Pope, P. L. Scott, and R. S. Shaw, "The chaotic behavior of the leaky faucet," Phys. Lett. A **110**, 399–404 (1985).

[4]J. Wisdom, S. J. Peale, and F. Mignard, "The chaotic rotation of Hyperion," Icarus **58**, 137–152 (1984).

[5]M. Berry, "The unpredictable bouncing rotator: A chaology tutorial machine," in Dynamical Systems: A Renewal of Mechanism, edited by S. Diner, D. Fargue, and G. Lochak (World Scientific, Singapore, 1986), pp. 3–12.
[6]A. Wolf and T. Bessoir, "Diagnosing chaos in the Space Circle," Physica D **50**, 239–258 (1991).
[7]P. Holmes, "Poincaré, celestial mechanics, dynamical-systems theory and 'chaos'," Phys. Rep. **193**, 137–163 (1990).
[8]S. De Souza-Machado, R. W. Rollins, D. T. Jacobs, and J. L. Hartman, "Studying chaotic systems using microcomputer simulations and Lyapunov exponents," Am. J. Phys. **58**, 321–329 (1990).
[9]J. D. Farmer, E. Ott, and J. A. Yorke, "The dimension of chaotic attractors," Physica D **7**, 153–180 (1983).
[10]E. Ott, C. Grebogi, and J. A. Yorke, "Controlling chaos," Phys. Rev. Lett. **64**, 1196–1199 (1990); Y. Braiman and I. Goldhirsch, "Taming chaotic dynamics with weak periodic perturbations," *ibid.* **66**, 2545–2548 (1991).

Experiment on the physics of the PN junction

A. Sconza, G. Torzo, and G. Viola
Dipartimento di Fisica Galileo Galilei, Università di Padova, via Marzolo 8-35131 Padova, Italy

(Received 4 May 1992; accepted 21 May 1993)

Simple apparatus, suitable for an undergraduate laboratory, allows precise measurements of the forward characteristics of Si and Ge "transdiodes" at different temperatures in the range 150–300 K. The experimental results are used to obtain a fairly accurate value of the universal constant e/k (elementary charge to Boltzmann constant ratio) and of the energy gap of Si and Ge.

I. INTRODUCTION

A simple experiment on the physics of the PN junction may be carried out in undergraduate laboratory courses, providing a determination of both the universal constant e/k (i.e., elementary charge to Boltzmann constant ratio) and of the energy gap E_g of the semiconductor material the junction is made of. In the experiment we assume the junction to be well described by the ideal diode equation

$$I=I_0[\exp(eV/kT)-1], \tag{1}$$

where I is the current and V is the voltage applied to the junction, e is the elementary charge, k is the Boltzmann constant, T is the absolute temperature, and I_0 is the inverse current (i.e., the current extrapolated for large negative V values), that is strongly dependent on the temperature and on the energy gap E_g of the semiconductor material.

While real diodes only approximately obey Eq. (1), the ideal behavior is well followed[1] by transistors whose collector and base are kept at the same voltage (this configuration is commonly named *diode connected transistor* or *transdiode).* Therefore we will use transdiodes as the best approximation to ideal diodes.

The experiment consists in measuring the forward characteristic of Si and Ge transdiodes, at various constant temperatures in the range $150\ \text{K} < T < 300\ \text{K}$. At any given temperature the semilogarithmic plot of the collector current I_c vs the base-emitter voltage V, for $V \gg kT$, is a straight line from which we may extract two quantities of interest: its slope equals e/kT, so that, knowing the working temperature, we may obtain a value for the universal constant e/k, and the intercept gives the value of the inverse current I_0. The value of the energy gap for the transdiode semiconductor material may be derived from the temperature dependence of I_0.

In Sec. II we briefly recall the theoretical model that justifies Eq. (1), discuss the dependence $I_0(T,E_g)$ of the inverse current on the temperature and on E_g, as well as the temperature dependence of the energy gap $E_g(T)$, and we explain the procedure used to derive the energy gap.

In Sec. III we describe the experimental apparatus, and in Sec., IV we discuss the results obtained using two Si transistors and one Ge transistor.

II. THEORY

The current–voltage relationship of the ideal PN junction, originally derived by Shockley,[2] and described by Eq. (1), follows from the assumption that the total current is the sum of two contributions: a forward current $I_F = I_0 \exp(eV/kT)$ due to the majority carriers that overcome the junction potential barrier, and an inverse current I_0 due to the minority carriers. If V is the voltage of the anode (P) with respect to the cathode (N), the barrier height *decreases* with positive V values while it *increases* with negative values: this explains the rectifying behavior of the junction.

The current of majority carriers (electrons from N to P region, and holes from P to N region) depends exponentially on the voltage V applied to the junction, owing to the Boltzmann factor that gives the probability for a carrier to have an energy higher than the *effective* potential barrier across the depletion layer.

The inverse current is due to the thermally generated minority carriers that diffuse into the depletion layer, where they are accelerated by the local electric field. As long as V is not too large, I_0 depends only on the minority

